CHALMERS


**Internal Report 06:04**

# LES OF MIXED CONVECTION BOUNDARY LAYER UNDER INFLUENCE OF RADIATION

**DARIOUSH G. BARHAGHI, LARS DAVIDSON**

*Division of Fluid Dynamics, Department of Applied Mechanics*
CHALMERS UNIVERSITY OF TECHNOLOGY
Göteborg, Sweden, October 2006

# LES OF MIXED CONVECTION BOUNDARY LAYER UNDER INFLUENCE OF RADIATION

DARIOUSH G. BARHAGHI, LARS DAVIDSON
Division of Fluid Dynamics, Department of Applied Mechanics
Chalmers University of Technology
SE-412 96 Göteborg, Sweden

# Contents

## Abstract

Mixed convection boundary layer in a vertical channel is studied using Large-eddy simulation. A constant heat flux boundary condition is applied to one of the channel walls while the other wall is kept insulated. The Grashof and Reynolds numbers based on the wall heat flux and the channel width are $Gr_W = 9.4 \cdot 10^7$ and $Re_W = 5080$. Owing to the large temperature difference between the hot wall and the inlet air, the governing equations are solved using two different approaches. In the first approach Boussinesq approximation considering constant properties is employed. In the other one, the equations with variable properties are used. A consequence of the hot wall high temperature is the radiation heat transfer which is also taken into account. It is shown that about $10\%$ of the heat is transferred via radiation. In the previous simulations (Barhaghi & Davidson (2006*b*)), due to capturing unphysical temperatures near the inlet, a blend of the central difference scheme and Van-Leer scheme in combination with a wiggle detector was used and large discrepancies between the simulations and the measurements detected. It was found that the dissipative effect of the blend scheme had nearly destroyed the turbulence close to the inlet. Therefore new simulations is carried out using the pure central difference scheme for the velocity field. It is shown that the turbulence is preserved at the inlet and contrary to the previous simulations, the results show a more grid independent behavior. However, the remained discrepancies between the simulations and measurements suggest that the inlet boundary condition is the main reason for the differences.

# Nomenclature

## Latin Symbols

| | |
|---|---|
| $D_e$ | length characteristic, $= 2W$ |
| $g$ | gravitational acceleration |
| $k$ | thermal conductivity of air |
| $P$ | pressure |
| $P_{u_i u_j}$ | production term in the Reynolds stress equations |
| $P_{u_i t}$ | production term in the turbulent heat flux equations |
| $P_{tt}$ | production term in the temperature variance equation |
| $q''_w$ | wall heat flux, $= 449 W/m^2$ |
| $T$ | temperature |
| $T_b$ | bulk temperature, $= T_{in}$ |
| $T_f$ | film temperature, $(T_h[K] + T_c[K])/2$ |
| $T_h$ | hot wall local temperature |
| $T_{in}$ | temperature of air at the inlet of the channel, $= 18.6^o C$ |
| $t$ | time |
| $\Delta t$ | computational time step |
| $U$ | stream-wise direction velocity |
| $U_b$ | bulk velocity |
| $W$ | width of the channel |
| $x$ | stream-wise axis |
| $y$ | wall normal axis |
| $z$ | span-wise axis |
| $\Delta x^+$ | computational cell length in terms of viscous units in the stream-wise direction |
| $y^+$ | distance of the wall adjacent node from the channel wall in terms of viscous units |
| $\Delta z^+$ | computational cell length in terms of viscous units in the span-wise direction |

## Greek Symbols

| | |
|---|---|
| $\beta$ | coefficient of expansion, $1/T_f[K]$ |

| | |
|---|---|
| $\varepsilon$ | channel walls emissivity |
| $\phi$ | general variable |
| $\mu$ | dynamic viscosity of air |
| $\mu_{SGS}$ | turbulent SGS viscosity |
| $\nu$ | kinematic viscosity of air, $\mu/\rho$ |
| $\rho$ | density of air |

## Dimensionless quantities

| | |
|---|---|
| $Gr_W$ | Grashof number, $g\beta q''_w W^4/\nu^2 k$ |
| $Re_W$ | Reynolds number, $U_b W/\nu$ |
| $Nu$ | local Nusselt number, $q''_w D_e/k(T_w - Tb)$ |
| $Pe$ | Peclet number, relative strength of convection and diffusion, $\rho V/(\Gamma/\delta)$ |

# 1 Introduction

Natural convection heat transfer exists in a number of industrial applications including reactors, and heat exchangers. An extensive study of this kind of boundary layer including both experiments and numerical simulations can be found in the literature. The results of these investigations have shown substantial differences between the conventional forced convection and natural convection boundary layers. However, there are still some aspects on which there is no general consensus among the researchers. On the other hand, the influence of natural convection in case of mixed convection boundary layers for moderate ratios of Reynolds to Grashof number is believed to be crucial. So appropriate modeling of this type of boundary layer demands further understanding of this flow (see Hanjalić (1994)).

Pure natural convection boundary layer on a vertical flat plate is studied experimentally in Tsuji & Nagano (1988). A unique feature of this flow is the production of turbulence in the region close to the wall which has large influence on the turbulent flow regime in the vicinity of the wall. In forced convection boundary layers, it is the Reynolds shear stress which contributes to the production of turbulence, whereas in natural convection boundary layer, it can be a sink term in the inner part of the boundary layer where the velocity gradient is positive. Consequently, the buoyancy production takes over the role of the source term and compensates for the production deficit due to the Reynolds shear stress. However, the results of the LES of natural convection boundary layer on a vertical cylinder in Barhaghi *et al.* (2006) does not completely comply with the findings of the mentioned experiment in the region close to the wall.

In order to appropriately model the turbulent flows to which the contribution of the natural convection is important, the length scale over which buoyancy expresses itself should be well understood. By assuming different level of interactions between the buoyancy and turbulent momentum, different modeling approaches can be considered. Study of the effect of the buoyancy on the turbulence budget of mixed convection boundary layer in a vertical infinite channel in Davidson *et al.* (2003)

shows that the buoyancy is only an important term in the momentum equation but not the stress equations. Mixed convection boundary layers in the presence of radiative heat transfer is also investigated in Wang *et al.* (2004).

Barhaghi & Davidson (2006*b*) made Large-eddy simulations according to one of the configurations of the above mentioned work to study the development of the boundary layer. Due to large Peclet numbers in the computational cells, a blend of the central difference scheme and Van-Leer scheme was used to avoid the spurious temperature and velocity fluctuations or the so called computational wiggles. Also at the channel inlet, instantaneous DNS results of a fully developed channel was prescribed. However, it was shown that the scheme had nearly destroyed the turbulent fluctuations at the inlet. This was speculated to be the reason why the experimental results were substantially different compared to the simulations.

In order to find out weather or not the so called blend scheme is the reason why the results show different behavior, new simulations are carried out applying the central difference scheme to the velocities and using the blend scheme only for the temperature.

## 2 Geometry and Grid Configuration

Figure 1 represents the buoyancy aided channel flow configuration which is in accordance to the experimental configuration in Wang *et al.* (2004). Two different grids with resolutions of $322 \times 66 \times 50$ (hereafter coarse grid) and $482 \times 66 \times 66$ (hereafter fine grid) in the $x$, $y$ and $z$ directions, respectively, are used to carry out the computations. The spatial resolution for the coarse grid, along the hot wall, is $\Delta z^+ < 45$ and $\Delta x^+ < 80$ in the span-wise and stream-wise directions. For the fine grid, the corresponding values are $\Delta z^+ < 33$ and $\Delta x^+ < 50$. In both cases $y^+ < 0.6$ for the wall adjacent node and $9\%$ stretch factor is used in the wall-normal ($y$) direction.

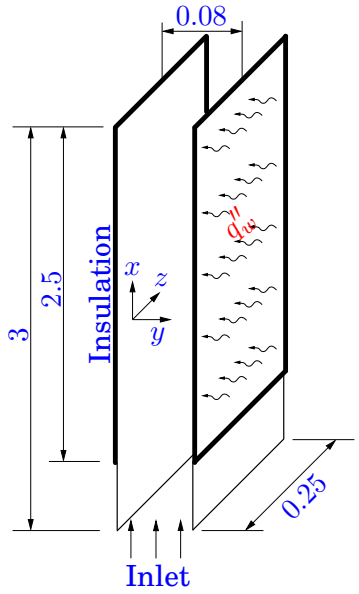


Figure 1: Computational geometry configuration. All the dimensions are in meter.

## 3 Numerical Method

Applying constant heat flux boundary condition on the hot wall causes the temperature of the hot wall to raise in the stream-wise direction. From the primary computations, it was found that the temperature difference between the hot wall and the inlet air raises to as high as $100^oC$. The first consequence of the high temperature difference in the flow is the ambiguity of the Boussinesq approximation validity. Thus, the Navier-Stokes and the energy equations are not only solved using Boussinesq approximation, but they are solved considering variable properties including varying density, viscosity, conductivity and specific heat. All the properties are extracted from thermodynamical tables and fourth order polynomial equations are fitted on them assuming they are independent of pressure. These equations are used in the finite volume code in order to estimate the properties.

### 3.1 Finite volume approach

A conventional finite volume method is used to solve the three-dimensional continuity, Navier-Stokes and temperature equations with the above mentioned characteristics. Space filtering is applied to the equations with constant properties. However, Favre averaged equations are solved in the case with the variable properties. The dynamic subgrid-scale model of Germano *et al.* (1991) is used to model the small eddies. The Second-order Crank-Nicolson scheme is used to discretize all the equations in time. In order to avoid the spurious fluctuations that occur in cells with the Peclet number $|Pe| > 2$, a blend of the central difference scheme with deferred correction (see Dahlström (2003)) and Van-Leer scheme in conjunction with a wiggle detector is used to discretize the temperature equation in space. However, the pure central difference scheme is used to discretize the velocity equations. The reason is that in the simulations of Barhaghi & Davidson (2006*b*), it was observed that the blend scheme had nearly destroyed the turbulence fluctuations at the inlet. The turbulence destruction is a consequent of the fact that it is almost impossible to differentiate between the turbulence fluctuations and the spurious ones in the case of the velocities. Thus, the scheme may incorrectly filter (dissipate) the turbulence instead of the spurious fluctuations. Fortunately, in the case of the temperature, it is easy to recognize a wiggle. A wiggle in this case is defined to be the local minima or maxima or when the temperature in a cell is higher or lower than the maximum or minimum boundary values (inlet and walls), respectively.

The numerical procedure is based on an implicit, fractional step technique with a multi-grid pressure Poisson solver and a non-staggered grid arrangement. The pressure Poisson equation in case of the constant property equations reads:

$$\frac{\partial^2 P}{\partial x_i \partial x_i} = \frac{\rho}{\Delta t} \frac{\partial u_i^*}{\partial x_i} \tag{1}$$

where $u_i^*$ is the intermediate velocity in the fractional step solution procedure (see Davidson & Peng (2003) for details). In the variable prop-

erty case, considering the continuity equation, the Poisson equation for pressure reads:

$$\frac{\partial^2 P}{\partial x_i \partial x_i} = \frac{1}{\Delta t}\left(\frac{\partial \rho}{\partial t} + \frac{\partial \rho u_i^*}{\partial x_i}\right) \tag{2}$$

### 3.2 Boundary Conditions

As it is depicted in Figure 1 the channel left wall is kept insulated for $x > 0.5\ m$. At the right wall, constant heat flux boundary condition, $q''_w = 449\ W/m^2$, is applied. However, these boundary conditions are modified considering radiation heat transfer. Air temperature and the Reynolds number are $T_{in} = 18.6^o C$ and $Re_W = 5080$. The Grashof number is $Gr_W = g\beta q''_w W^4/(\nu^2 k) \approx 9.4 \cdot 10^7$ where $W = 0.08\ m$. So, the Grashof to Reynolds number ratio is $Gr_W/Re_W^2 \approx 3.6$, suggesting that the buoyancy effects are as important as the inertial effects.

The instantaneous DNS results of a fully developed channel are prescribed as the inlet boundary condition. At the outlet, convective boundary condition has been used for velocities and temperature. Cyclic boundary condition is applied in the span-wise ($z$) direction.

Another consequence of the hot wall high temperature is that the radiation heat transfer becomes significant. The radiation heat transfer is assumed to be two-dimensional meaning that span-wise variation of the radiation is neglected. Provided the radiosity equation for each grid cell on the channel walls, the Gauss-Seidel method is used to solve for the surface radiosities at each time step. The emissivity of the channel walls is set to $\varepsilon = 0.125$ (from the experimental data) and both inlet and outlet are assumed to be black body surfaces.

### 3.3 Radiation Heat Transfer

Since the temperature of the heated wall increases considerably, the radiation heat transfer comes into effect. The radiation heat transfer is assumed to be two-dimensional meaning that the span-wise variation

of the radiation is neglected. Figure 2 shows the schematic diagram of the vertical channel while its walls are segmented by two-dimensional strips. In this figure, $l$ and $r$ stand for the left and the right wall respectively and $nj-1$ is the number of cells in the stream-wise direction.

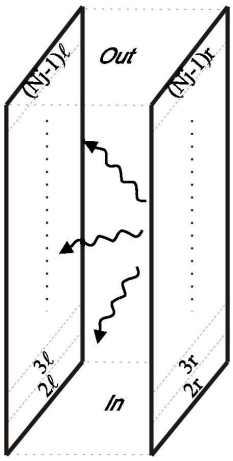


Figure 2: Schematic diagram of the radiation heat transfer in the channel.

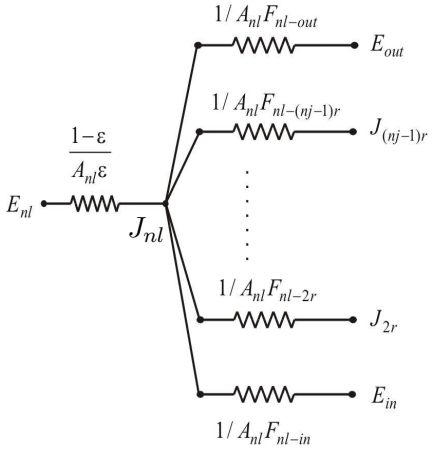


Figure 3: Equivalent circuit diagram of the radiation heat transfer in the channel.

The equivalent circuit diagram of the radiation exchange between the $n^{th}$ strip on the left wall ($n = 2...nj-1$), the right wall strips, the inlet and the outlet is shown in Figure 3. The inlet and the outlet are assumed to be black bodies and the area weighted average temperature at the outlet is assumed to be the temperature of the surface.

By considering this diagram for the left or insulated wall and a similar diagram for the right or heated wall, the governing equations for the left and the right wall cell radiosities, $J_{nl}$ and $J_{nr}$, read:

$$\begin{aligned} J_{nl}\left(\tfrac{1}{1-\varepsilon}\right) - \quad & \textstyle\sum_{m=2}^{nj-1}\left(J_{mr}F_{nl-mr}\right) = \\ & E_{nl}\left(\tfrac{\varepsilon}{1-\varepsilon}\right) + E_{out}F_{nl-out} + E_{in}F_{nl-in} \end{aligned} \tag{3}$$

$$\begin{aligned} J_{nr}\left(\frac{1}{1-\varepsilon}\right) - \quad & \sum_{m=2}^{nj-1}\left(J_{ml}F_{nr-ml}\right) = \\ & E_{nr}\left(\frac{\varepsilon}{1-\varepsilon}\right) + E_{out}F_{nr-out} + E_{in}F_{nr-in} \end{aligned} \tag{4}$$

In which, $F_{nl-mr}$ is the view factor between the $n^{th}$ strip on the left wall and $m^{th}$ strip on the right or heated wall, $\varepsilon = 0.125$ is the emissivity of the walls and $E$ is the black body emission of a segment where the name of the segment is written as the subscript.

Regarding Figure 4, view factors between the channel wall strips (considering two dimensionality) are calculated by Equations 5 and 6.

$$\begin{cases} F_{R-L} = \frac{\sqrt{(n+1)^2\ A^2+1} - 2\sqrt{n^2\ A^2+1} + \sqrt{(n-1)^2\ A^2+1}}{2A} \\ A = H/W,\ n = |y_r - y_l|/H \end{cases} \tag{5}$$

$$\begin{cases} F_{R-I} = \frac{W}{H}\left[\left(\frac{A-\sqrt{1+A^2}}{2}\right) - \left(\frac{A'-\sqrt{1+A'^2}}{2}\right)\right] \\ A = h/W,\ A' = (h-H)/W \end{cases} \tag{6}$$

Equations 3 and 4 are composed of $2 \times (nj-1)$ equations that are solved by a Gauss-Seidel method at each time step. Provided the radiosities, the radiated and irradiated heat flux at each time step can be calculated using Equation 7.

$$\begin{cases} q''^{\ irrad}_{nl} & = \frac{E_{nl}-J_{nl}}{(1-\varepsilon)/\varepsilon} \\ q''^{\ rad}_{nr} & = \frac{E_{nr}-J_{nr}}{(1-\varepsilon)/\varepsilon} \end{cases} \tag{7}$$

The irradiated heat flux will be used as the actual heat flux of the left wall (instead of the zero value) and the radiated heat flux will be subtracted from $q''_w$ to account for the effect of the radiation heat transfer.

# 4 Results

After assessing fully developed flow condition by tracking the time variation of the Nusselt number at different heights, sampling is started. In

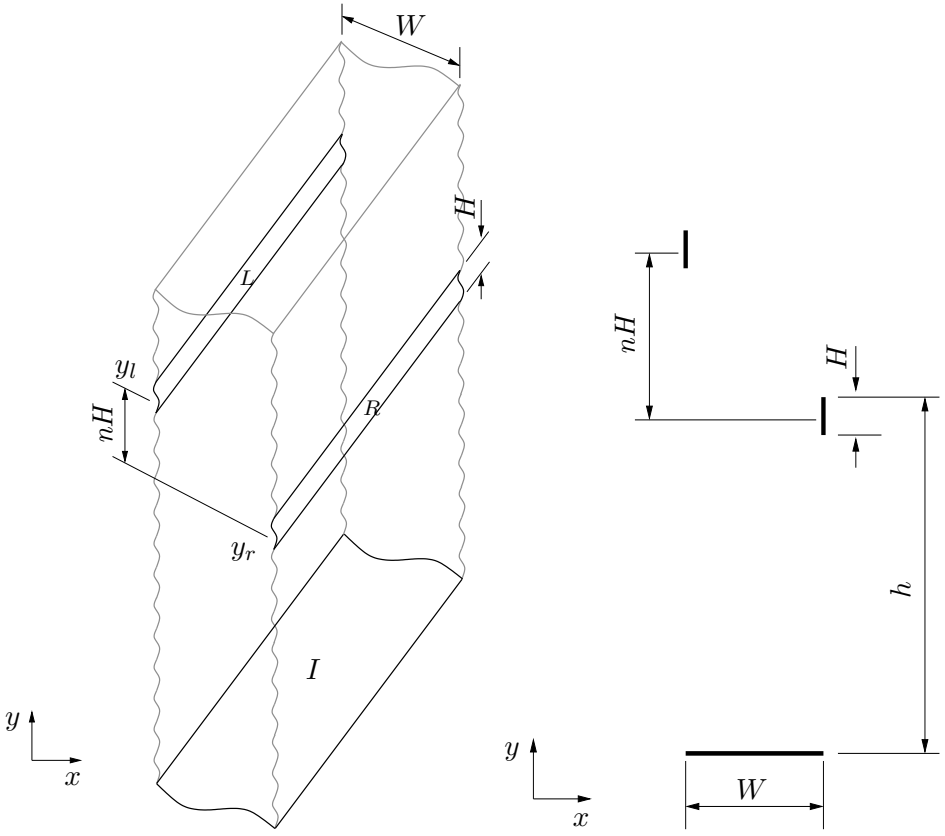


(a) Three dimensional configuration.

(b) Two dimensional configuration.

Figure 4: The geometrical dimensions between the channel wall segments (strips) to calculate the view factor between them and the channel inlet and outlet.

the constant property case, time averaged samples are obtained which is defined as $\langle\phi\rangle = 1/T \int_0^T \phi$. In the variable property case, however, Favre averaged samples are obtained which by considering time averaging definition is $\widetilde{\phi} = \langle\rho\phi\rangle/\langle\rho\rangle$. In the following, unless otherwise stated, the results of the case with the fine grid considering variable properties and including radiation are presented.

## 4.1 Wiggle Detector and Inlet Boundary Condition

Figure 5 shows the effect of the wiggle detector on the shear stress variations at the entrance region of the channel. It can be seen in Figure 5(b) that this scheme has dampened the turbulent shear stress greatly. However, the turbulent shear stress is almost perfectly preserved in Figure 5(a) because of using the pure central difference scheme for the velocity equations. The small fraction of the turbulent shear stress which is dissipated is due to the SGS viscosity. This viscosity decreases the magnitude of the turbulent shear stress slightly.

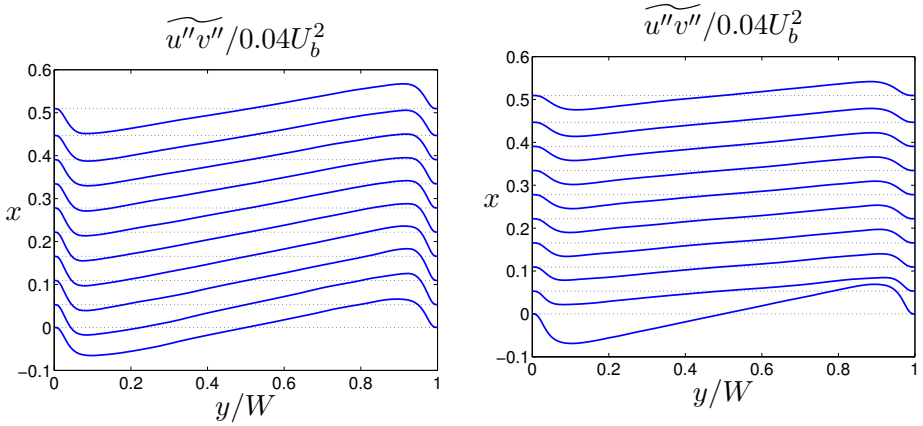


(a) Central difference scheme

(b) Blend scheme with wiggle detector

Figure 5: The turbulent shear stress near the inlet of the channel for the fine mesh and variable properties using different discretization schemes for the velocity equations.

The reason why the turbulent shear stress is dampened can be seen in Figure 6 which shows the proportion of the central difference (value 1) and Van-Leer schemes (value 0).

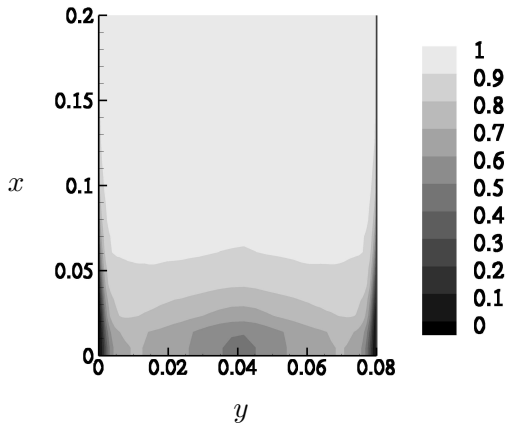


Figure 6: Contours of scheme usage ratio near the entrance of the channel.

Although a small fraction of the blend scheme is Van-Leer, it is enough to dissipate the velocity fluctuations and hence reducing the magnitude of the turbulent shear stress. Except for the inlet, wiggle detector has mostly used the central difference scheme. This can also be understood from Figure 5(b) which shows that the shear stress is preserved at $x > 0.05\ m$.

## 4.2 Grid Dependency Assessment

Figure 7 compares the velocity and the temperature profiles for different grid resolutions, considering constant fluid properties. When the blend scheme is applied to the velocities, the results are even more grid dependent (see Barhaghi & Davidson (2006*b*)) than the above results.

Results of the variable property computations are also shown in Figure 8. The results in this case are rather grid independent.

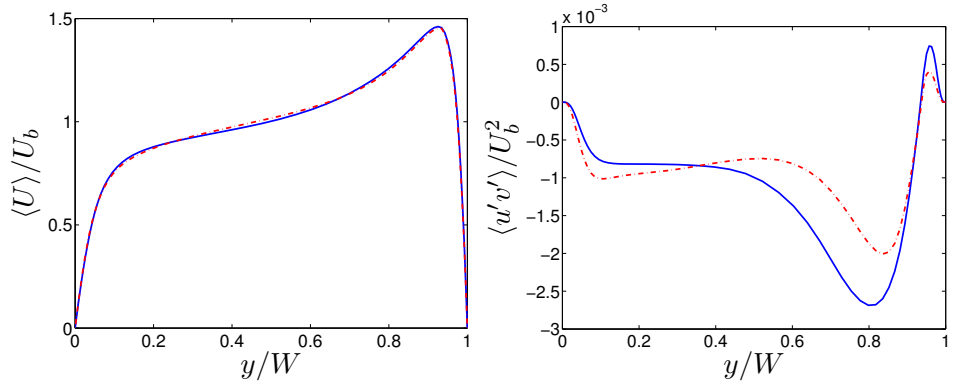


(a) Normalized velocity profile (b) Turbulent shear stress

Figure 7: Velocity and turbulent shear stress profiles at $x = 2.5m$ for constant property computations. —— : fine mesh; -·-·- : coarse mesh.

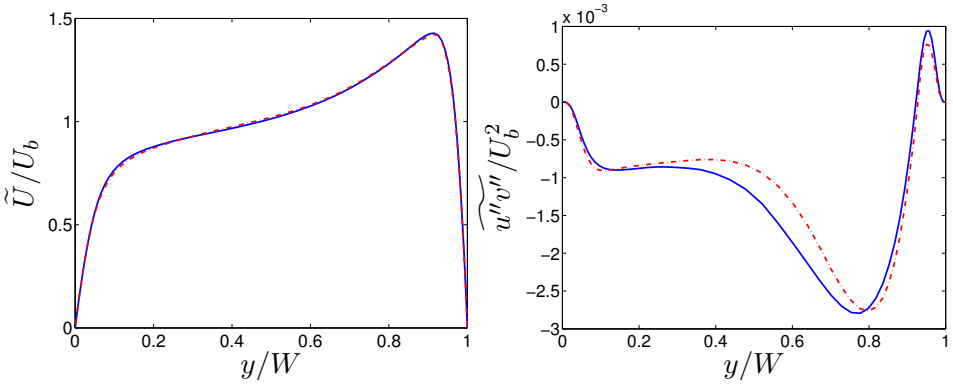


(a) Normalized velocity profile (b) Turbulent shear stress

Figure 8: Velocity and turbulent shear stress profiles at $x = 2.5m$ for variable property computations. —— : fine mesh; -·-·- : coarse mesh.

### 4.3 Property Dependency Assessment

The mean velocity and turbulent shear stress in the cases of the constant and variable property computations are compared in Figure 9. Surprisingly, the results of the constant property computations show a close behavior to the results of the variable property computations even at this high temperature difference.

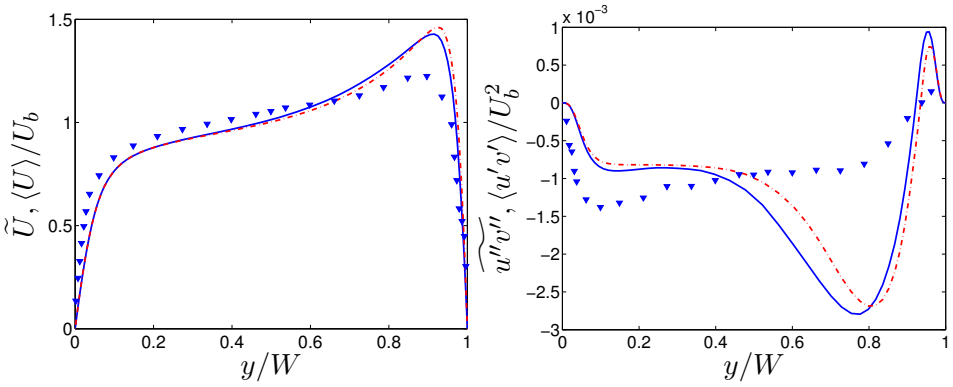


(a) Normalized velocity profile

(b) Turbulent shear stress

Figure 9: Variable and constant property results comparison at $x = 2.5m$. —— : variable property; -·-·- : constant property; ▽ : Experimental results of Wang *et al.* (2004).

The largest differences between the turbulent shear stresses of the variable and constant property computations lie in the region between $0.5 \leq y \leq 0.8$. This region lies almost in the middle of the channel where the convective terms are larger compared to the regions close to the wall. This is probably why the density differences play more important role in this region.

### 4.4 Radiation Effect

Radiation is calculated at each time step and it is added as a sink/source term in the cells adjacent to the hot/insulated wall. Figure 10(a) com-

pares the velocity profiles of two cases where the radiation heat transfer is considered and neglected, respectively. In the both cases, it is assumed that the flow properties remain constant and computations are performed on the coarse grid.

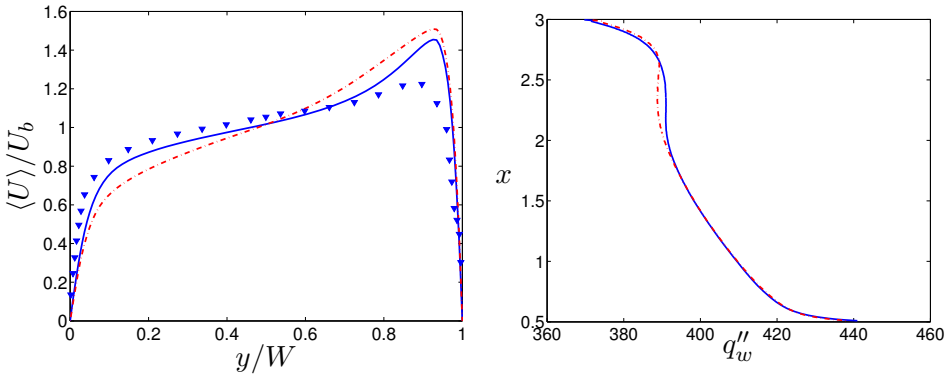


(a) Velocity profile. ——: with radiation; - - -: neglecting radiation; ▽ : measurements

(b) Hot wall heat flux. ——: Fine grid; - - -: coarse grid

Figure 10: Effect of radiation heat transfer on velocity and the remaining heat flux on the hot wall.

Figure 10(b) shows the conductive hot wall heat flux on both fine and coarse grids considering variable properties. Since the total heat flux on the hot wall is $449\ W/m^2$, on average more than $10\%$ of the heat flux is transferred via radiation. Therefore, the radiation heat transfer is an important aspect of this problem and can not be neglected.

## 4.5 Mean Flow Parameters

Velocity profiles were shown in the previous sections. Another two important parameters are temperature and Nusselt number whose variations are shown in Figure 11. Once again, the effect of the radiation can be seen in Figure 11(a) in which the variation of the temperature along the insulated wall is shown. This temperature would remain constant,

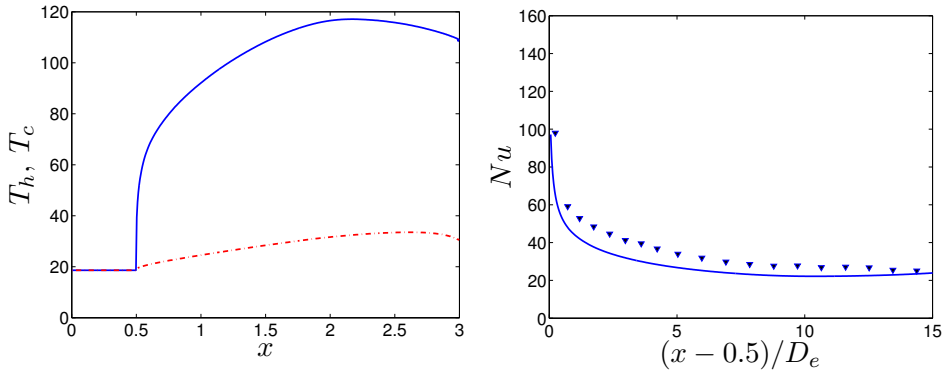


(a) Temperature variations. ——: Hot wall; - - -: insulated wall.

(b) Nusselt number. ——: Computations; ▽: measurements. $D_e = 2 \cdot W$

Figure 11: Temperature variations along the hot and insulated wall and Nusselt number variations along the hot wall considering variable properties and radiation.

equal to the inlet temperature ($T_b = 18.6^oC$), if the effect of radiation was neglected. The reason why temperature falls slightly at $x > 2.5\ m$ is that the outlet is considered to be a black body surface. Hence, it is assumed that each cell on the walls exchanges heat with outlet via radiation assuming the outlet temperature to be equal to the bulk temperature at the outlet.

Figure 11(b) compares the variation of the computed and measured Nusselt numbers along the hot wall for $x > 0.5\ m$. The predicted Nusselt number is smaller than the measured one. This difference is especially large in the lower part of the channel where $0.5 < x < 0.8$.

## 4.6 Reynolds Stresses

Aside from the Reynolds shear stress which is shown above, all other normal Reynolds stresses, turbulent heat fluxes and temperature fluctuations are plotted in Figure 12.

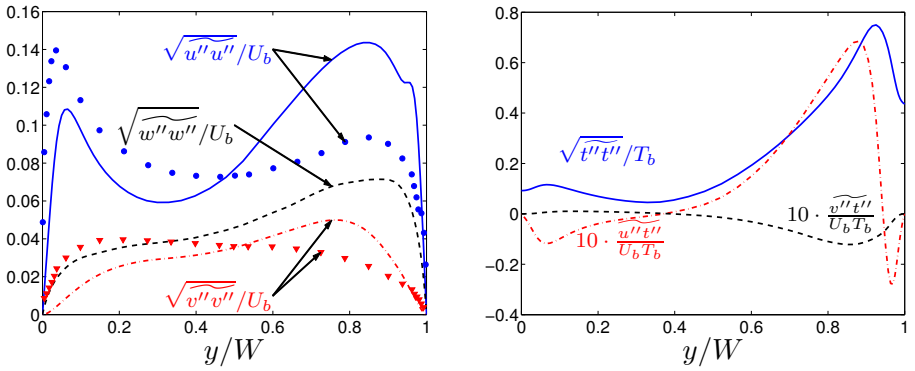


(a) Normal fluctuations.

(b) Turbulent heat fluxes and temperature fluctuations.

Figure 12: Reynolds stresses, turbulent heat fluxes and temperature fluctuations at $x = 2.5\ m$.

Similar to the turbulent shear stress, discrepancies between the computations and the measurements in the case of the normal stresses are large. In case of the temperature fluctuations and turbulent heat transfer, no experimental data are available for comparison.

# 5 Boundary Layer Development

In this section, the boundary layer development is studied by investigating the behavior of the mean flow and turbulent parameters at different heights of the vertical channel. Velocity and temperature profiles at different heights are shown in Figure 13.

It can be seen in Figure 13(a) that the fluid acquires higher velocity magnitudes close to the hot wall as it moves downstream. Temperature profiles also show that the boundary layer becomes thicker and thicker as it develops in the channel passage.

The two important parameters that play an essential role in the turbulent boundary layer development are the turbulent shear stress ($\widetilde{u''v''}$)

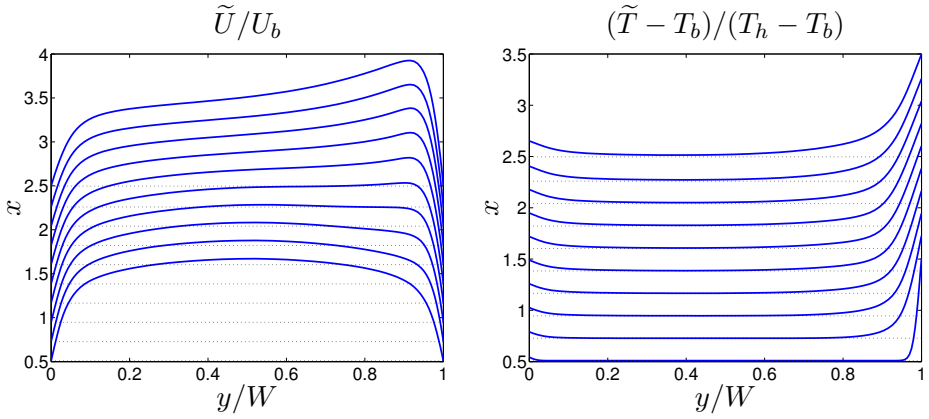


(a) Velocity profiles.

(b) Temperature profiles.

Figure 13: Velocity and temperature profiles across the channel at different heights.

and the wall normal turbulent heat flux ($\widetilde{v''t''}$) which are shown in Figure 14.

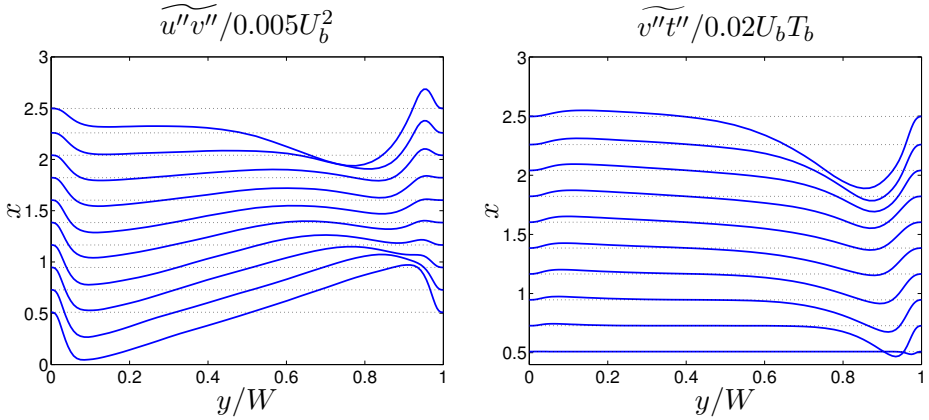


(a) Turbulent shear stress.

(b) Wall normal turbulent heat flux.

Figure 14: $\widetilde{u''v''}$ and $\widetilde{v''t''}$ profiles across the channel at different heights.

At $x = 0.5\ m$ where the heat flux boundary condition is applied, symmetrical profile of a fully developed channel flow can be observed in case of the turbulent shear stress. Since temperature boundary layer is just about forming, $\widetilde{v''t''}$ is zero at this height. Near the hot wall, as the boundary layer grows, $\widetilde{u''v''}$ is reduced. As the flow goes upward, $\widetilde{u''v''}$ in the inner part of the boundary layer ($y/W > 0.9$), eventually becomes zero from where it starts to attain positive values. However, in the outer part of the boundary layer, the negative shear stress attains larger magnitudes since the production of shear stress, $P_{uv} = -\widetilde{v''v''}\partial\widetilde{U}/\partial y + g\beta\widetilde{v''t''}$, is negative (due to positive velocity gradient and negative wall normal heat flux). But, in the inner part of the boundary layer, the production of shear stress due to $\widetilde{v''v''}$ is larger than the other negative term resulting in positive shear stress in the inner boundary layer.

By considering the major production term of the wall normal turbulent heat flux, $P_{vt} = -\widetilde{v''v''}\partial\widetilde{T}/\partial y$, it can be concluded that due to the positive temperature gradient and consequently negative $P_{vt}$, $\widetilde{v''t''}$ attains negative values close to the hot wall.

Since $\widetilde{v''v''}$ plays an important role in the productions of $\widetilde{u''v''}$ and $\widetilde{v''t''}$, its evolvement as the boundary layer grows is shown in Figure 15(a). $\widetilde{v''v''}$ is symmetrical at the location where the temperature boundary layer begins. As the boundary layer evolves, $\widetilde{v''v''}$ attains larger/smaller values close to the hot/insulated wall.

The Reynolds shear stress together with the stream-wise turbulent heat flux have significant impacts on $\widetilde{u''u''}$ whose variations across the channel at different heights are shown in Figure 15(b). This can be understood by considering the production of $\widetilde{u''u''}$ whose major terms are $-2\widetilde{u''v''}\partial\widetilde{U}/\partial y$ and $2g\beta\widetilde{u''t''}$. In the inner boundary layer at the hot wall, due to the negative velocity gradient and positive shear stress, the former term is positive. However, the latter term is negative due to the negative $\widetilde{u''t''}$ (see Figure 16(a)). Nevertheless, as the magnitude of the production due to the shear stress is larger, the total production remains positive. In the outer boundary layer, where $\widetilde{u''v''}$ and $\widetilde{v''t''}$ are negative and $\widetilde{t''t''}$, the velocity and temperature gradients are positive, $P_{ut} = -\widetilde{v''t''}\partial\widetilde{U}/\partial y - \widetilde{u''v''}\partial\widetilde{T}/\partial y + g\beta\widetilde{t''t''}$ remains positive which results

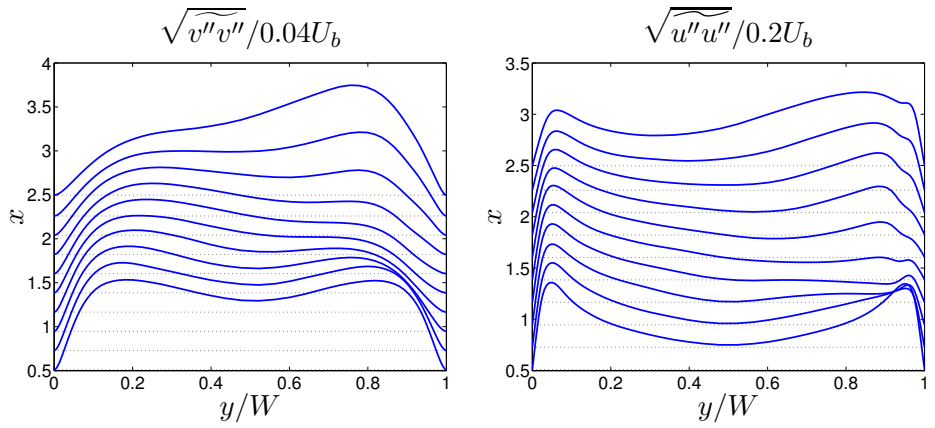


(a) Wall normal Reynolds stress.

(b) Stream-wise Reynolds stress.

Figure 15: $\widetilde{v''v''}$ and $\widetilde{u''u''}$ profiles across the channel at different heights.

in a positive $\widetilde{u''t''}$. Consequently, in the outer layer, the positive and large $\widetilde{u''t''}$ makes the $\widetilde{u''u''}$ large in the boundary layer.

Figure 16(b) shows the trend of $\widetilde{t''t''}$ at different heights of the channel. It can be seen that as the boundary layer along the hot wall grows $\widetilde{t''t''}$ attains larger values owing to the negative $\widetilde{v''t''}$ and positive temperature gradient which makes its production, $P_{tt} = -2\widetilde{v''t''}\partial\widetilde{T}/\partial y$, to remain positive and increase along the channel as $|\widetilde{v''t''}|$ increases.

In turn, $\widetilde{t''t''}$, $\widetilde{v''t''}$ and $\widetilde{u''v''}$ affect the stream-wise turbulent heat flux. Positive $\widetilde{u''v''}$, results in a negative $\widetilde{u''t''}$ in a small region close to the hot wall as $P_{ut}$ is negative in that region. However, beyond this region, as the turbulent shear stress changes sign, $\widetilde{u''t''}$ attains positive values in major portion of the boundary layer.

# 6 Conclusions

Boundary layer development in a vertical channel is studied using Large-Eddy simulation. Dynamic model is used as the SGS model. This model

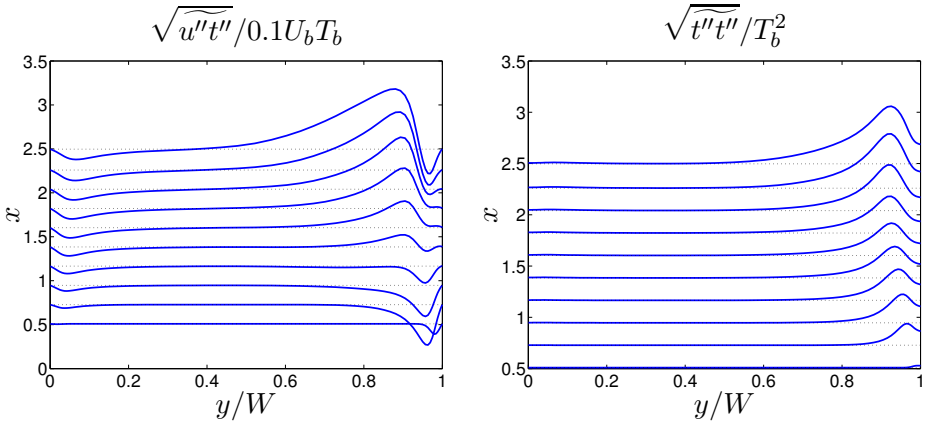


(a) Stream-wise turbulent heat flux.

(b) Temperature fluctuations.

Figure 16: $\widetilde{u''t''}$ and $\widetilde{t''t''}$ profiles across the channel at different heights.

is able to capture the backscattered energy by yielding negative SGS-viscosity (see Figure 17).

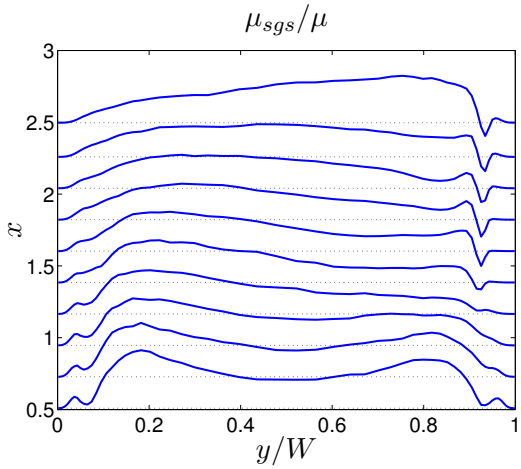


Figure 17: $\langle \mu_{sgs} \rangle$ profiles across the channel at different heights.

A so called wiggle detector scheme is used but is applied only to the

temperature because in Barhaghi & Davidson (2006*a*) it was found that the use of this scheme for velocities had dampened the prescribed turbulence at the inlet substantially.

Due to relatively high temperature differences, the full governing equations with variable properties are solved. The Boussinesq approximation yields reasonable results although the temperature differences reaches to as high as $100^oC$. Unfortunately, even full equations result in considerably different mean flow and turbulence parameters compared to the measurements. A comparison of the computed and measured results shows that the measured profiles at $x = 2.5\ m$ are more similar to the computed profiles at lower heights, i.e. the computed profiles at $1.5\ m \leq x \leq 2\ m$. This suggests that the boundary layer in the case of the experiment has developed slower than the computations. This in turn can be interpreted as if the flow at the inlet has been laminar or has had a very low turbulence level in the case of the measurements. Thus, the larger measured Nusselt numbers can also be a consequence of the inlet conditions.

Finally, it can be concluded that prescribing a uniform flow at the inlet may significantly improve the computational results.

# 7 Acknowledgments

This work is partly financed by the Swedish Research Council which is gratefully acknowledged.

# References

BARHAGHI, D. G. & DAVIDSON, L. 2006*a* LES of mixed convection boundary layer between radiating parallel plates. In *Turbulence, Heat and Mass Transfer 5* (ed. K. Hanjalić, Y. Nagano & S. Jakirlić), pp. CD–ROM. New York: begell house, Inc.

BARHAGHI, D. G. & DAVIDSON, L. 2006*b* Natural convection boundary layer in a 5:1 cavity (submitted for publication). *Physics of Fluids* .

BARHAGHI, D. G., DAVIDSON, L. & KARLSSON, R. 2006 Large-eddy simulation of natural convection boundary layer on a vertical cylinder. *International Journal of Heat and Fluid Flow* **27**, 811–820.

DAHLSTRÖM, S. 2003 Large eddy simulation of the flow around a high-lift airfoil. PhD thesis, Dept. of Thermo and Fluid Dynamics, Chalmers University of Technology, Göteborg, Sweden.

DAVIDSON, L., ČUTURIĆ, D. & PENG, S.-H. 2003 DNS in a plane vertical channel with and without buoyancy. In Turbulence Heat and Mass Transfer 4 (ed. K. Hanjalić, Y. Nagano & M. Tummers), pp. 401–408. New York, Wallingford (UK): Begell House, Inc.

DAVIDSON, L. & PENG, S.-H. 2003 Hybrid LES-RANS: A one-equation SGS model combined with a $k - \omega$ model for predicting recirculating flows. *International Journal for Numerical Methods in Fluids* **43**, 1003–1018.

GERMANO, M., PIOMELLI, U., MOIN, P. & CABOT, W. H. 1991 A dynamic subgrid-scale eddy viscosity model. *Physics of Fluids A* **3**, 1760–1765.

HANJALIĆ, K. 1994 Achievements and limitations in modelling and computation of buoyant turbulent flows and heat transfer. In *10th Int. Heat Transfer Conference*. Brighton, UK.

TSUJI, T. & NAGANO, Y. 1988 Turbulence measurements in a natural convection boundary layer along a vertical flat plate. *International Journal of Heat and Mass Transfer* **31** (10), 2101–2111.

WANG, J., LI, J. & JACKSON, J. D. 2004 A study of the influence of buoyancy on turbulent flow in a vertical plane passage. *International Journal of Heat and Fluid Flow* **25** (3), 420–430.